JACS
JOURNAL OF THE AMERICAN CHEMICAL SOCIETY
Article
pubs.acs.org/JACS

Polycatenar Ligand Control of the Synthesis and Self-Assembly of Colloidal Nanocrystals

Benjamin T. Diroll,[†,⊥,▽] Davit Jishkariani,[†,‡,▽] Matteo Cargnello,[†,#] Christopher B. Murray,[*,†,§] and Bertrand Donnio[*,‡,∥]

[†]Department of Chemistry, University of Pennsylvania, Philadelphia, Pennsylvania 19104, United States
[‡]Complex Assemblies of Soft Matter Laboratory (COMPASS), UMI 3254, CNRS-Solvay−University of Pennsylvania, Bristol, Pennsylvania 19007, United States
[§]Department of Materials Science and Engineering, University of Pennsylvania, Philadelphia, Pennsylvania 19104, United States
[∥]Institut de Physique et Chimie des Matériaux de Strasbourg (IPCMS), UMR 7504, CNRS−Université de Strasbourg, 67034 cedex 2, Strasbourg, France

Supporting Information

ABSTRACT: Hydrophobic colloidal nanocrystals are typically synthesized and manipulated with commercially available ligands, and surface functionalization is therefore typically limited to a small number of molecules. Here, we report the use of polycatenar ligands derived from polyalkylbenzoates for the direct synthesis of metallic, chalcogenide, pnictide, and oxide nanocrystals. Polycatenar molecules, branched structures bearing diverging chains in which the terminal substitution pattern, functionality, and binding group can be independently modified, offer a modular platform for the development of ligands with targeted properties. Not only are these ligands used for the direct synthesis of monodisperse nanocrystals, but nanocrystals coated with polycatenar ligands self-assemble into softer *bcc* superlattices that deviate from conventional harder close-packed structures (*fcc* or *hcp*) formed by the same nanocrystals coated with commercial ligands. Self-assembly experiments demonstrate that the molecular structure of polycatenar ligands encodes interparticle spacings and attractions, engineering self-assembly, which is tunable from hard sphere to soft sphere behavior.

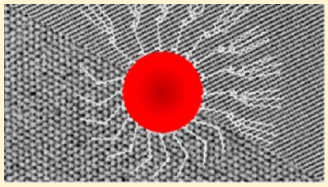

INTRODUCTION

Research on ligands bound to colloidal nanocrystals (NCs) is maturing into the significance that has long been achieved in other fields of chemistry. Ligand coatings can be used to control solubility,[1−4] self-assembly,[5−8] thermal stability,[9,10] optical properties,[11] electronic conduction,[12] catalysis,[13] magnetism,[14] medical therapies,[15] and NC synthesis.[16] With some important exceptions, the toolset of available ligands is limited to commercial sources, leaving space for synthetic design of tailored ligands. Indicating the potential of ligand design, DNA-coated NCs in aqueous media demonstrate ligand-controlled self-assembly and sensing.[17−19] Similarly, precise matching of inorganic metal chalcogenide ligands with CdSe NCs yields films of exceptional conductivity.[20]

For NCs in hydrophobic media, ligands are typically paraffinic alkyl amines, phosphines, thiols, or carboxylic or phosphonic acids. These remain invaluable, but the fields of liquid crystals and supramolecular chemistry show the structural complexities and practical utility achievable through thoughtful exploitation of organic chemistry. Recent efforts have demonstrated coating of colloidal NCs with dendritic or liquid-crystalline ligands[5−7,14,21−32] that influence the self-assembly behavior of NC−ligand hybrids including thermally switchable[5,33] or photoswitchable structures.[34] Colloidal NCs coated with various types of mesomorphous ligands have demonstrated self-assembly into many liquid crystalline and crystalline assemblies.[5−7,28−36] Most efforts rely on postsynthetic ligand exchange, although direct syntheses of colloidal NCs have been reported with Au NCs near room temperature.[35−37] In these examples, the size distribution of NCs is large, indicating that tight control over the NC size has until now not been achieved in direct synthesis with noncommercial ligands.

Here, we demonstrate the direct synthesis of monodisperse NCs using polycatenar ligands. These ligands[14] are composed of an anchoring group to bind the particle surface, a branched tail of alkyl chains to enhance solubility, and a triazole ring linking the two components together. Our modular synthetic strategy accesses polycatenar ligands with independently tunable peripheral chain substitution and functionality and diverse anchoring groups to bind NCs of different chemical compositions. To demonstrate their wide utility, we use these ligands to synthesize a broad range of nanocrystals including cadmium and lead chalcogenides, ZnO, Fe_2O_3, InP, and Au.

Direct synthesis, as opposed to ligand exchange, has both advantages and limitations: it is more demanding of material stability but enables ligand-dependent control of the resulting NCs and their properties with unambiguous surface termination. In ligand-exchange reactions, sterically hindered ligands

Received: May 14, 2016
Published: July 29, 2016

DOI: 10.1021/jacs.6b04979
J. Am. Chem. Soc. 2016, 138, 10508−10515

Scheme 1. Synthesis of the Various Libraries of Polycatenar Ligands Arranged According to Their Functionalities[a]

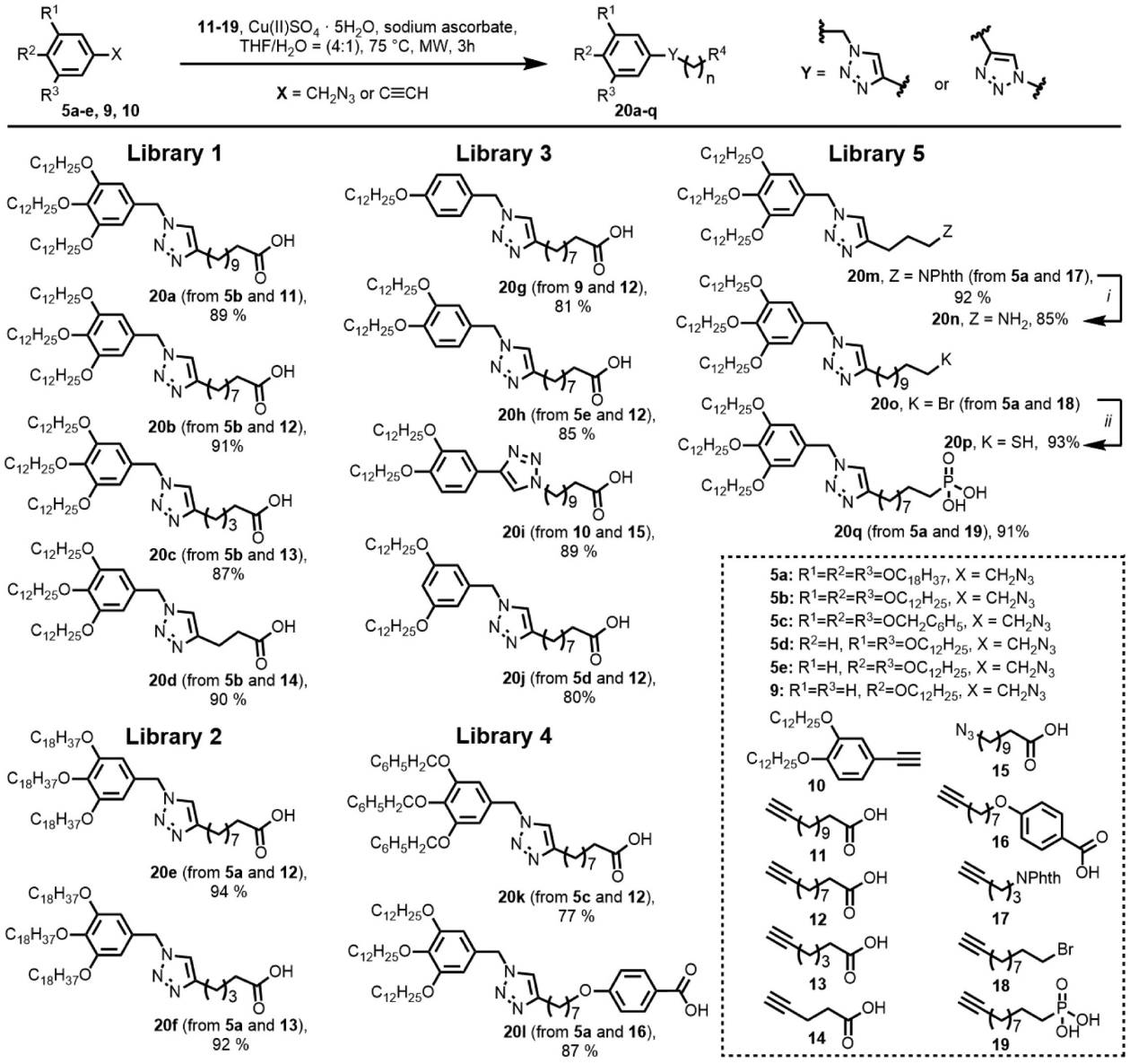

[a]Reagents and conditions: (i) Hydrazine, THF, 60 °C, 4 h; (ii) thiourea, EtOH, reflux, 12 h. The complete characterization of ligands **20a−q**, as well as the synthesis of the precursors **5a−e**, **9**, **10**, and **16** and all other intermediates **1a−c** through **8** are described in detail in Supporting Information.

are particularly problematic candidates to bind to particle surfaces, and the ligand shells may be incompletely exchanged. Nonetheless, ligand molecules may function noninnocently in reactions, so we also perform ligand exchange with polycatenar ligands on selected NCs.

For optimized reactions, direct synthesis with polycatenar ligands yields NCs with monodispersity comparable to similar syntheses using commercial reagents. Self-assembly into single-component and binary nanocrystal superlattices (BNSLs) demonstrates the excellent monodispersity of NCs prepared by direct synthesis with polycatenar ligands. The longer organic ligand shells strongly affect self-assembly, as NC behavior becomes softer, diverging further from the organizing principles of hard spheres. In single-component systems, polycatenar ligands induce a size-dependent transition from close-packed hard structures (*fcc* or *hcp*) to softer *bcc* superlattices. The BNSL phases that are observed in these softer NC superlattices largely conform to the predicted trends of recent theoretical work on the phase diagram for binary colloidal NCs with soft interaction potentials.[38]

EXPERIMENTAL SECTION

Full details of materials, synthetic procedures, and characterization methods are contained in the Supporting Information.

RESULTS AND DISCUSSION

Ligand Synthesis and Design. Ligands used in the direct synthesis of NCs must survive the thermal and chemical conditions of reactions in addition to stabilizing NCs against aggregation. Building from the known stability of alkyl and phenyl ethers in NC synthesis, the peripheral functionalization of the polycatenar ligands is achieved via Williamson ether synthesis (Scheme 1).[39] Thermal analysis indicates the success of this approach: decomposition of the ligand material occurs at >300 °C, similar to oleic acid (See Supporting Information

DOI: 10.1021/jacs.6b04979
J. Am. Chem. Soc. 2016, 138, 10508−10515

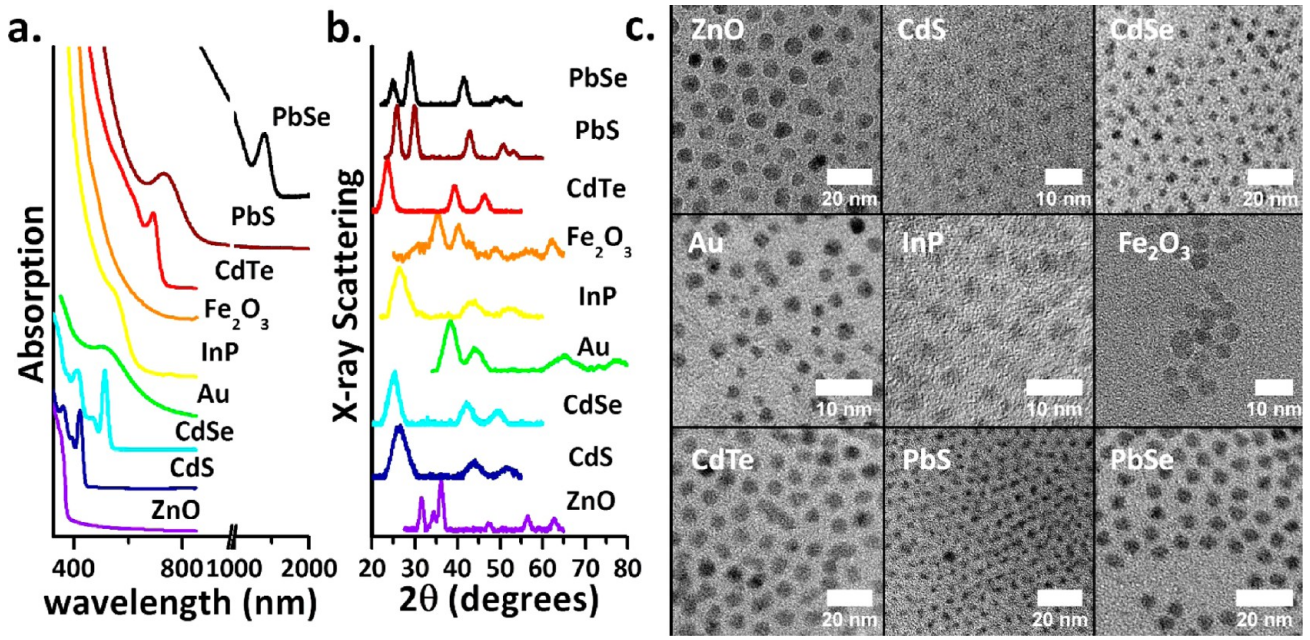

Figure 1. (a) Optical absorption spectra, (b) X-ray diffraction patterns, and (c) TEM micrographs of NCs prepared by direct synthesis with polycatenar ligands. CdS, InP, Fe_2O_3, PbS, and PbSe samples are capped with ligand **20b**. The CdTe sample is capped with ligand **20q**, CdSe with **20d**, ZnO with **20i**, and Au with **20n**.

Figure S1). The five libraries of ligands in Scheme 1 are synthesized in a modular approach. For one-half, peripheral units of lipophilic alkyl-decorated polyhydroxbenzoates are functionalized as azides (**5a**−**e**, **9**). For the other component, surface-anchoring groups with carboxylic or phosphonic acid, amine, and thiol binding groups are terminated with alkynes (**11**−**19**). To synthesize the final targets (**20a**−**20q**), we relied upon the Huisgen "click" cylcloaddition chemistry.[40] To study the influence of the triazole ring orientation and the presence of benzylic methylene unit, we also prepared corresponding phenyl acetylene **10** as model system (making **20i**).[39] This late-stage functionalization permits independent variation of the ligand structure, for example, number and length of chains and anchoring functionality, which enables a study of the influence of such parameters on NC properties and allows broader compatibility with NCs of diverse chemistries.

The ligands **20a**−**q** fall into five libraries that address changes of ligand design. Library 1 consists of ligands **20a**−**d** with different anchoring spacer lengths but identical (C12) alkyl substitution pattern, and library 2 (**20e**−**f**) consists of longer (C18) homologues. Ligands with different number and substitution pattern of alkyl end groups **20g**−**j**, together with an example of a ligand with differently oriented triazole unit, **20i**, are shown in library 3. Library 4 consists of ligands where we introduce aromatic rings either at the periphery (as end groups), **20k**, or the anchoring unit, **20l**. Noncarboxylate ligands (**20n**, **20p**−**q**) are gathered in library 5.

Synthesis of Nanocrystals. The results of several syntheses of different NCs are shown in Figure 1. Reaction conditions are typically chosen with little adjustment from literature practice, replacing commercial fatty acid, amine, or phosphonic acid ligands with equimolar amounts of polycatenar analogs (Full details in Supporting Information). Figure 1a shows the UV to near-IR absorption spectra, and Figure 1b shows the X-ray diffraction patterns for examples of each material. The optical spectra are similar to reported work, indicating formation of the desired NC compositions. For the semiconductor NCs, which exhibit quantum confinement, first absorption features reflect inhomogeneous broadening of electronic structure, primarily due to size dispersion: the first absorption features of CdS, CdSe, CdTe, PbS, and PbSe NCs are comparable to previous reports of monodisperse semiconductor NCs.[41−43] X-ray crystal structures observed in direct synthesis with polycatenar ligands are consistent with stable polymorphs for each of the materials. Au NCs show a *fcc* structure, ZnO NCs exhibit the wurtzite crystal structure, whereas CdS, CdSe, CdTe, and InP exhibit zinc blende crystal structures, and lead chalcogenides form in the rock-salt structure. The X-ray structures of maghemite (Fe_2O_3) and magnetite (Fe_3O_4) are not sufficiently different for phase assignment in this case. The assignment to the fully oxidized maghemite phase is made on the basis of past literature, which has shown that small crystallites are easily oxidized into maghemite.[44]

TEM micrographs confirming the formation of NCs appear in Figure 1c. TEM confirms the low polydispersity apparent from optical absorption spectra for many samples. The standard deviation of diameters for the cadmium and lead chalcogenides was <10% of the average diameter in all cases, unless noted. Synthetic conditions for InP (2.6 ± 0.5 nm) and Fe_2O_3 (4.4 ± 0.9 nm) NCs in particular likely require further optimization; however, ZnO samples (7.0 ± 0.8 nm) with polycatenar ligands were sufficiently monodisperse to self-assemble into *hcp* superlattices. Although the ZnO inorganic cores are more polydisperse than typically required for self-assembly, the organic coating counteracts inhomogeneity of the inorganic component and fosters ordered assembly.

Thermal analysis, FT-IR, and NMR experiments confirm that intact polycatenar ligands coat the surface of NCs. Thermogravimentric analysis experiments confirm the increase in organic weight fraction for **20b**-capped 2.8 nm CdSe (45 wt %) compared with oleate-capped 2.8 nm CdSe NCs (34 wt %). FT-IR experiments show the absence of olefinic C−H bonds (Supporting Information Figure S6) in polycatenar-capped

DOI: 10.1021/jacs.6b04979
J. Am. Chem. Soc. 2016, 138, 10508−10515

NCs and ^{1}H NMR of 2.4 nm **20d**-capped CdSe or **20a**-capped 7.0 nm ZnO, cleaned by precipitation five times to remove excess ligand, unambiguously shows NMR signals associated with the functional groups of **20d** or **20a**, respectively (Supporting Information Figures S7 and S8).

CdSe was used as a pilot system to study the effect of different ligands on NC synthesis. NCs of CdSe synthesized with polycatenar ligands show excellent monodispersity apparent from the absorption spectra in Figure 2. Under the same reaction conditions, the size of the resulting CdSe NCs varied from 2.4 to 6.0 nm according to the ligand that was used. As the ligand size increased, the resulting size of the NCs generally increased, although the relation is imperfect. This suggests that larger ligands suppress nucleation leading to fewer nuclei and larger NCs. Consistent with this view, the largest ligand **20e** yields large (>50 nm) prismatic NCs (see Supporting Information Figure S19). Not all ligands shown in Scheme 1 produced monodisperse CdSe NCs when used in pilot reactions. Reactions with ligands **20h** and **20j**, with distinct peripheral chain substitution, produce soluble CdSe NCs with an average size consistent with the trend of steric hindrance (reactions with 3,5-branched **20h** produced smaller NCs than with 3,4-branched **20j**) but insufficiently monodisperse to demonstrate long-range self-assembly. Monoalkyl (**20g**), triphenyl (**20k**), and benzoate-anchoring (**20l**) derivatives showed poor solubility in situ and resulted in polydisperse, frequently aggregated products. In particular, the distinction between branched and unbranched structures in NC solubility provides additional support for enhanced solubility of NCs incorporating ligands with branches.[45] When ligand exchange is performed on oleate-capped CdSe NCs, those exchanged with **20k**, containing phenyl peripheral functionality, become insoluble in hexane but remain soluble in toluene; those exchanged with the **20g** and **20l** are insoluble in nonpolar organic solvents such as hexanes, toluene, and chloroform. These experiments highlight the significant role of the ligand structure motifs in preserving solubility of the colloids during reactions.

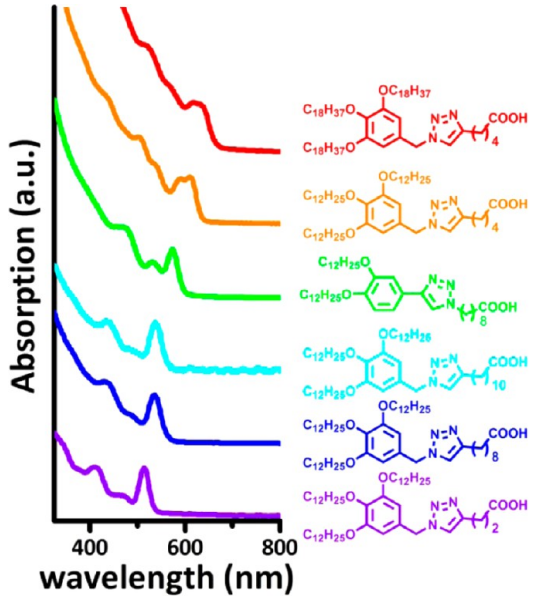

Figure 2. Visible absorption spectra of CdSe NCs synthesized with different polycatenar carboxylic acids as the ligands. The chemical structure of the ligand used in each synthesis is shown at right in the same color.

Single-Component NC Self-Assembly. Nanocrystals prepared by direct synthesis or coated through ligand exchange with polycatenar ligands showed size- and ligand-dependent self-assembly. To obtain self-assembled structures from hard spheres typically requires ≤5% diameter inhomogeneity and therefore self-assembly is a powerful demonstration of monodispersity. By softening differences of inorganic size, polycatenar ligands facilitate self-assembly into periodic single-component superlattices and BNSLs even in those cases (e.g., ZnO) where the nanocrystals would seem too polydisperse. Figure 3 shows typical self-assembly behavior of NCs with polycatenar ligands (more in Supporting Information). Figure 3a shows the (110) projection a *bcc* superlattice of **20b**-capped 2.8 nm CdSe, and Figure 3b shows the same projection for a superlattice of **20b**-capped 2.4 nm CdS nanocrystals. Larger NCs prepared by direct synthesis including (Figure 3c) **20i**-capped 7.0 nm ZnO and (Figure 3d) **20b**-capped 5.5 nm PbSe NCs self-assembled into hexagonally packed superlattices.

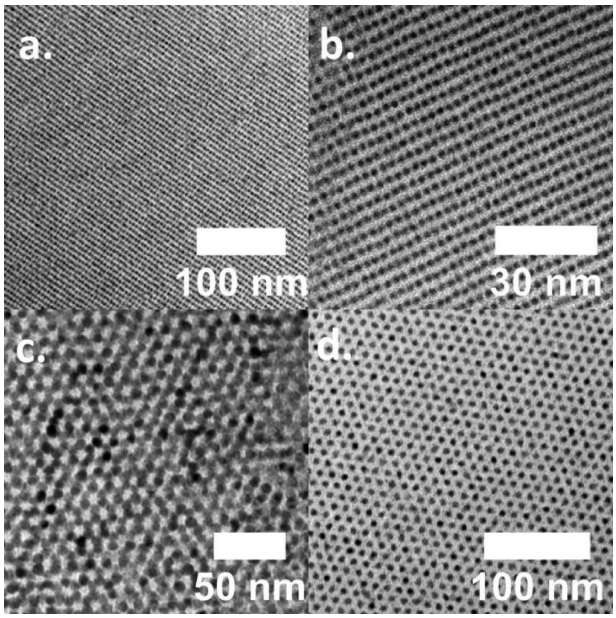

Figure 3. Projections along (001) of (a) *bcc* **20b**-capped 2.8 ± 0.2 nm CdSe, (b) **20b**-capped 2.4 ± 0.2 nm CdS, (c) *hcp* **20i**-capped 7.0 ± 0.8 nm ZnO, and (d) close-packed hexagonal monolayer of **20b**-capped 5.5 ± 0.4 nm PbSe NCs.

The observation of *bcc* superlattices, rather than a stable hard sphere phase, raises several lines of inquiry. In the remainder of Figure 4, we separately examine the influence of the ligands on the same size of NC, the effect of branching, and the use of the same ligands on NCs of different size. Figure 4a,b shows 2.8 nm CdSe NCs capped with ligand **20a**, which formed *bcc* assemblies, or oleic acid, which formed close-packed superlattices. TEM studies of CdSe samples showed that the effective solid state ligand length (defined as one-half of edge-to-edge distance) of polycatenar ligands used in this work varied from 1.4 nm (**20d**) to 2.2 nm (**20a**) compared with ∼1 nm for oleic acid. The larger spacings engineered with polycatenar ligands are critical for generating deviation from hard sphere behavior. Using a ligand with two branches rather than three hardens self-assembly behavior: Figure 4c,d show polymorphism in **20i**-

DOI: 10.1021/jacs.6b04979
J. Am. Chem. Soc. 2016, 138, 10508−10515

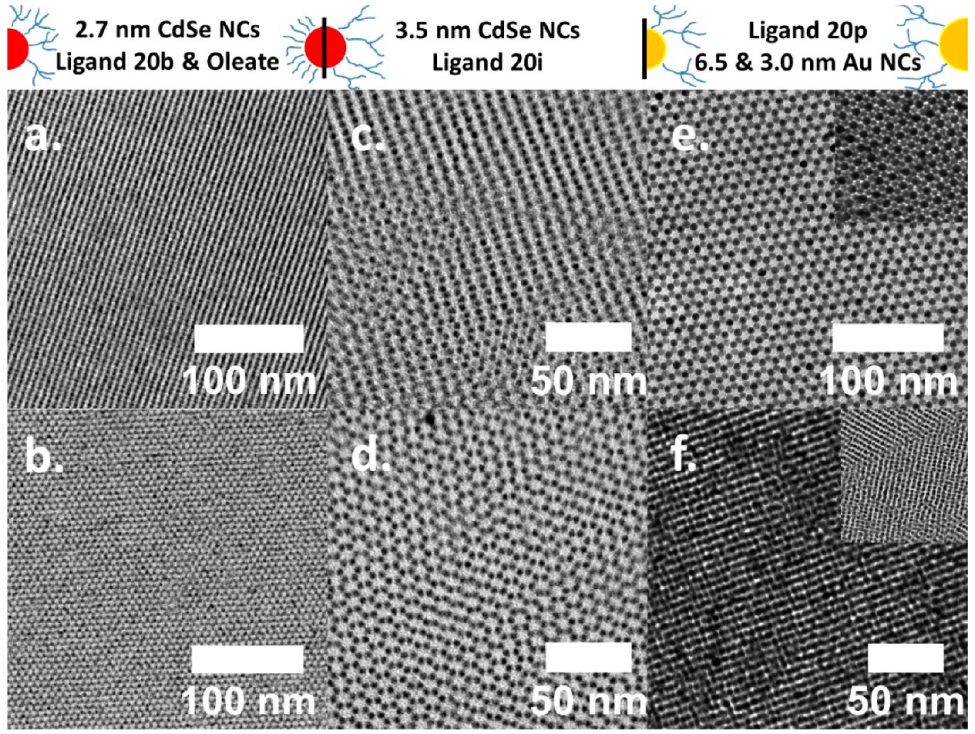

Figure 4. (a) Self-assembly, *bcc*-type, of 2.8 ± 0.2 nm CdSe NCs prepared by direct synthesis with ligand **20a**, (b) *hcp*-type assembly of 2.8 ± 0.2 nm CdSe NCs prepared by synthesis with oleic acid ligands, (c, d) 3.5 nm CdSe NCs capped with **20i** polycatenar ligand self-assembled into *hcp*, *fcc*, and *bcc* superlattices, (e) *hcp* superlattice of **20p**-capped 6.5 ± 0.4 nm Au NCs (inset shows an *fcc* assembly of the same sample, and (f) **20p**-capped 3.0 ± 0.4 nm Au NCs in a *bcc* superlattice (inset shows another region of *bcc* superlattices for the sample, including a characteristic twin boundary).

capped 3.5 nm CdSe NC superlattices, for which the ligand shell thickness is ∼1.8−1.9 nm. This suggests a turning point in the self-assembly behavior where the contribution of the organic material eclipses the contribution of the inorganic material to the total diameter of the organic−inorganic NC unit. A further demonstration is shown by **20p**-capped 6.5 and 3.0 nm Au NCs. The observed ligand layer thickness of **20p**-capped gold was larger than **20b**-capped semiconductors, presumably due to the larger number of binding sites and consequently greater ligand density. With a ligand of fixed length of 2.2 nm, 6.5 nm Au NCs show *hcp* and *fcc* superlattices (Figure 4e) and 3.0 nm Au NCs show *bcc* superlattices (Figure 4f). This strongly suggests that the large relative organic size of softer systems increasingly stabilizes the more open *bcc* structure. Indeed, *bcc* superlattices were observed exclusively from NCs with organic thickness greater than the particle radius, with all NCs larger than ∼4 nm showing hard *hcp* or *fcc* packing.

Previous work has claimed that *bcc* structures are observed for small (<3 nm) NCs with oleate ligands because the *bcc* structure reduces ligand frustration due to a highly symmetrical truncated octahedron shape of the Voronoi polyhedron.[46] NCs may also deviate from hard sphere behavior because they are not spheres: 7.5 nm oleate-capped PbSe nanocrystals form *bcc* structures, such as in Supporting Information Figure S26, but this represents the highest packing density structure for such truncated octahedra. In the case presented in this work, the observed behavior is dependent on the organic ligand choice, because the inorganic cores (e.g., in Figure 4a,b) are nearly identical in size, shape, and monodispersity, but the size of the organic layer is substantially different. (See comparison of SAXS and SANS in Supporting Information Figure S23)

A separate treatment of soft sphere behavior, which also offers a unified approach with BNSLs, is based on interparticle potentials of the form[38,47]

$$V_{jh}(r) = \varepsilon\left(\frac{\sigma_{jh}}{r}\right)^{p}$$

where σ_{jh} is the center-to-center distance of j and h NCs, r is interparticle distance, and ε is a scalar reflecting the strength of interaction. For potentials $p \leq 7$, the *bcc* phase also becomes stable.[47] Softness, judged from the size of organic shell relative to the inorganic core determined by TEM measurements,[48] maps intuitively onto different values of p. For samples in which the organic material is smaller than the inorganic core size, like **20p**-capped 6.5 nm Au NCs or oleate-capped 2.8 nm CdSe NCs, behavior is "hard" ($p > 7$), with the formation of *hcp* or *fcc* superlattices. For systems with organic coatings that are larger than the NC radius, including all NCs with diameters <4 nm with three-branch polycatenar ligands, exclusively *bcc* superlattices are observed. With two-chain **20i**-capped CdSe, polymorphism between *bcc*, *fcc*, and *hcp* phases is observed, suggesting similar energies of all three phases ($p \approx 7$). From self-assembly data, we conclude that engineering polycatenar ligands enables softer interparticle potentials ($p \leq 7$) than previous NC systems with commercial ligands.[48]

Binary NC Self-Assembly. In addition to single-component superlattices, BNSL structures, several of which are shown in Figure 5, are obtained by coassembly of two samples. More structures, including two binary liquid crystal phases and unidentified structures, are reported in the Supporting Information (see Figures S27−S35). The observed BNSLs encompass many structures observed in prior work including phases isostructural with CuAu, Cu_3Au, AlB_2, $NaZn_{13}$,

DOI: 10.1021/jacs.6b04979
J. Am. Chem. Soc. 2016, 138, 10508−10515

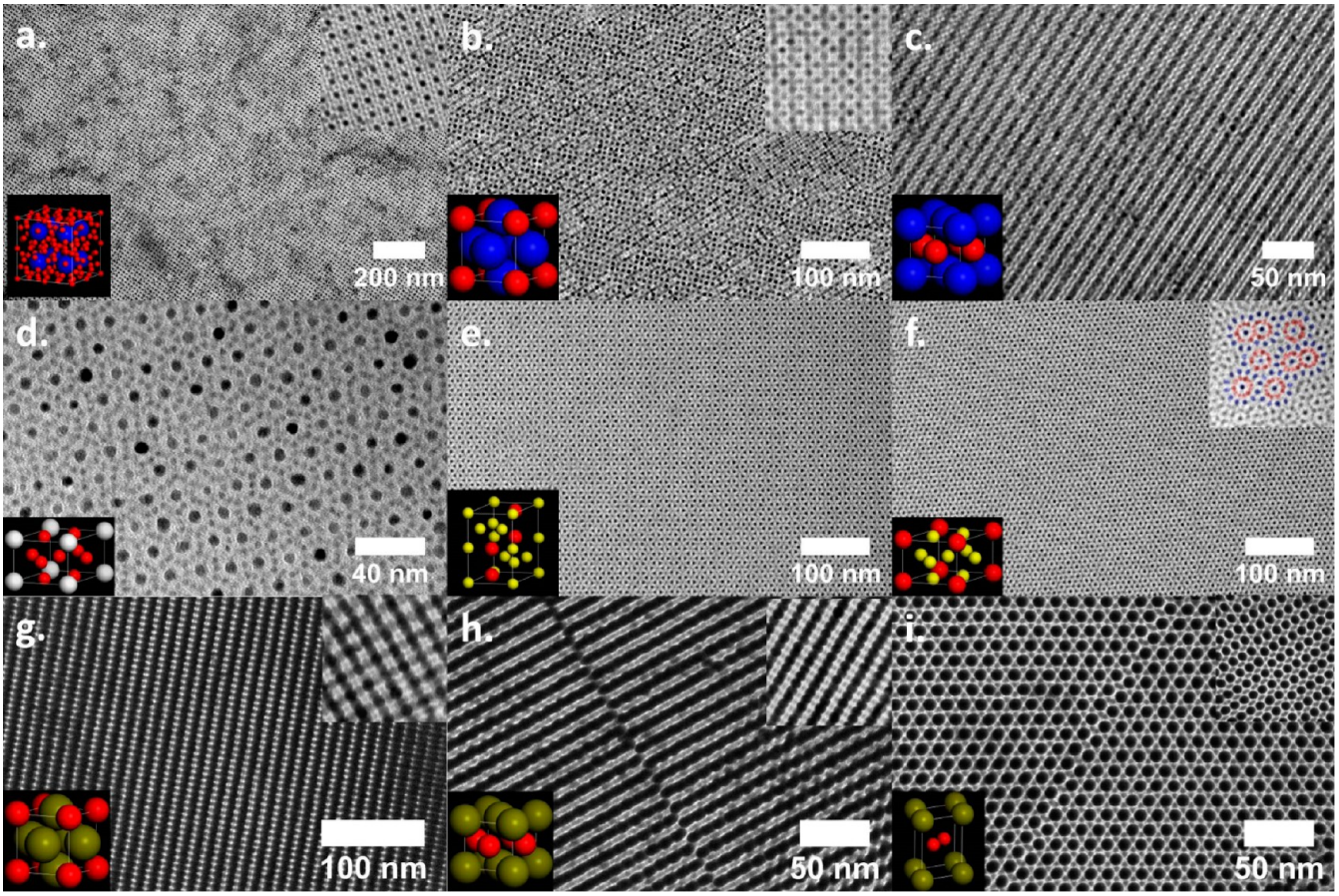

Figure 5. TEM micrographs of (a) $NaZn_{13}$, (b) Cu_3Au, and (c) CuAu BNSLs composed of different stoichiometries of **20b**-capped 5.5 nm PbSe and **20d**-capped 2.4 nm CdSe NCs capped with polycatenar ligands. (d) $CaCu_5$ BNSL composed of **20i**-capped 3.5 nm CdSe and **20i**-capped 7.0 nm ZnO NCs. (e) $MgZn_2$ and (f) $CaCu_5$ BNSLs composed of different stoichiometries of **20i**-capped 3.5 nm CdSe and **20b**-capped 2.4 nm CdS NCs. The colorized inset of (f) shows 12-fold symmetric defects, which occur in mixtures of the two NCs. (g) Cu_3Au-type, (h) CuAu-type, and (i) AlB_2-type BNSLs formed from different stoichiometries of oleate-capped 2.8 nm CdSe and **20p**-capped 6.5 nm Au NCs. Insets of panels g and h show images from other BNSL domains of the same type. Cartoons of the unit cell for each crystal structure are inset at the bottom left of the images.

$MgZn_2$, and $CaCu_5$.[49] Recent experimental[48] and theoretical[38,50] works conclude that soft sphere behavior induced by organic ligands increases the number of equilibrium BNSL phases, consistent with observed structural diversity.[49] The formation of several different BNSL structures using long polycatenar ligands allowed us to extend this analysis. Following Horst and Travesset,[38,50] the thermodynamics of BNSL phases are modeled by a modification of the power law equation above:

$$V_{jh}(r) = \varepsilon_{AA}\hat{\varepsilon}_{jh}\left(\frac{\sigma_{jh}}{r}\right)^{p}$$

where $\hat{\varepsilon}_{jh}$ represents interaction of the j and h NCs, assuming that $\hat{\varepsilon}_{AA} = 1$. Figure 6 shows relevant equilibrium phases for exponential values of $p = 6$ and $p = 12$ versus NC size ratio γ, defined as the diameter (inorganic core plus ligand shell) of the small NC divided by the diameter of the large NC.[50] Average values of inorganic diameters and ligand lengths are obtained via TEM imaging (see Table 1).

To map experimental results of this work onto the coordinate of $\hat{\varepsilon}_{AB}$, the best correlation between experiment and theory found in earlier results uses a coordinate of $c\gamma \cdot s_{AB}$, where c is a scalar (1.0 for $p = 12$; 0.85 for $p = 6$) and s_{AB} is the softeness asymmetry parameter defined as[50]

$$s_{AB} = \frac{\text{ligand shell thickness of small NC}}{\text{ligand shell thickness of large NC}}$$

We plot the experimental findings of this work in Figure 6 using colored dots, which indicate the BNSL structure. In general, the results are in substantial agreement with theoretical predictions, although there are points of difference. Our work shows previously noted preferences for nonequilibrium phases: where CsCl is predicted over a large parameter space, the similar CuAu is observed in our system.[38] Also, $MgZn_2$-type BNSLs, rather than $MgCu_2$, are found experimentally, although the energy and structure difference between these phases is very small, and we have therefore plotted them in the same color in Figure 6. Although the *bcc* phases observed in the single-component systems suggest a potential with $p < 7$ for smaller NCs, in the BNSLs achieved from combinations of these NCs, Figure 6 shows better agreement with a $p = 12$ exponent. This seems most likely because the potential between larger particles, one of the constituents of a binary system, is harder, as observed in single-component self-assembly. Most points fall within ± 0.1 in γ or s_{AB} (which also allows for measurement error) from the equilibrium lines for the relevant phase. For example, CuAu and $MgZn_2$ points fall close or within the equilibrium regions of CsCl and $MgCu_2$, respectively, and most other experimentally observed BNSLs are close to the

DOI: 10.1021/jacs.6b04979
J. Am. Chem. Soc. 2016, 138, 10508−10515

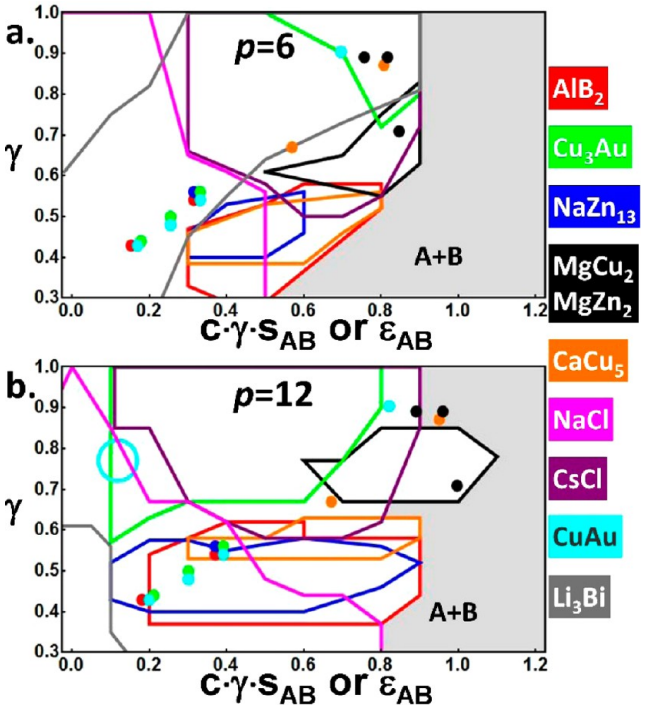

Figure 6. Equilibrium phases of BNSLs for (a) $p = 6$ and (b) $p = 12$, mapped as a function of size ratio (γ) versus interaction (ε_{AB}) or empirically measured softness asymmetry parameter (s_{AB}). The equilibrium regions of each phase, indicated by color at right, are shown with solid lines. The solid gray region represents the equilibrium state of phase separation of the two components. Dots represent experimentally observed BNSLs. Due to their similarity, the line for $MgCu_2$ and dots for $MgZn_2$ are plotted in the same color. In those cases of polymorphism from a given combination, the dots are offset slightly for visual clarity. The value of c is 0.85 in (a) and 1.0 in (b). Equilibrium lines from ref 50.

equilibrium regions for the observed phase. Where our data differs substantially from the theoretical equilibrium predictions is in the appearance of the Cu_3Au BNSLs, which appeared at much smaller values of γ and in the $p = 6$ case lower values of s_{AB}, than predicted. In several cases, in fact, Cu_3Au phases were observed at points in phase space, especially for $p = 6$, for which Li_3Bi BNSLs are the favored equilibrium phase. These data may provide additional information for the refinement of models of NC self-assembly and may hint at the necessity of adopting a more molecule-specific description of interparticle interactions in some cases.[51]

In summary, click reactions of diverse surface anchoring chemistries with branched lipophilic terminal groups access a library of new ligands for colloidal NCs. Our modular approach offers a way to bring organic functionality to inorganic NCs to control, in this case, solubility, interparticle spacings, and self-assembly behavior. This same approach may be expanded to offer templates for further conjugation, chirality, ligand segregation or patchiness, and electronic structure. Ligands synthesized in this study showed the thermal stability necessary for direct synthesis of NCs of several compositions yielding monodisperse NCs unambiguously functionalized with polycatenar ligands. We observe a size- and ligand-dependent transition from close-packed to open superlattice structures in line with theoretical predictions, and binary lattices self-assembled from NCs coated with polycatenar ligands hew reasonably well to the predicted equilibrium phases for BNSLs using a soft interparticle potential.

■ ASSOCIATED CONTENT

Supporting Information

The Supporting Information is available free of charge on the ACS Publications website at DOI: 10.1021/jacs.6b04979.

Additional synthesis procedures and characterization data of organic compounds and inorganic nanocrystals (PDF)

■ AUTHOR INFORMATION

Corresponding Authors

*cbmurray@sas.upenn.edu

*bdonnio@ipcms.unistra.fr

Present Addresses

[⊥]B.T.D.: Center for Nanoscale Materials, Argonne National Laboratory.

[#]M.C.: Department of Chemical Engineering, Stanford University.

Author Contributions

[▽]B.T.D. and D.J. contributed equally.

Notes

The authors declare the following competing financial interest: Aspects of this work have been included in a U.S. provisional patent filing No. 62/310047.

■ ACKNOWLEDGMENTS

The authors thank A. Travesset for helpful discussions and access to prepublication data and python scripts and K. Weigandt for assistance running SANS experiments. This work was supported by the CNRS-UPENN-SOLVAY through the Complex Assemblies of Soft Matter Laboratory (COMPASS),

Table 1. Tabulated Particle Sizes and Distances of NCs Forming BNSL Structures

large NCs	small NCs	d_{large} [a]	d_{small}	t_{large} [b]	t_{small}	γ [c]	s_{AB} [d]	BNSL(s)
oleate-CdSe	**20d**-CdSe	5.3	2.4	1.0	1.4	0.71	1.40	$MgZn_2$
20p-Au	**20d**-CdSe	6.5	2.4	2.2	1.4	0.48	0.64	CuAu,Cu_3Au
20p-Au	oleate-CdSe	6.5	2.8	2.2	1.0	0.44	0.45	CuAu, AlB_2, Cu_3Au[e]
20b-PbSe	**20d**-CdSe	5.5	2.4	2.0	1.4	0.55	0.70	$NaZn_{13}$, Cu_3Au, AlB_2, CuAu
20i-CdSe	**20b**-CdS	3.5	2.4	1.9	2.0	0.88	1.05	$CaCu_5$, $MgZn_2$
20i-ZnO	**20i**-CdSe	7.0	3.5	1.9	1.9	0.68	1.00	$CaCu_5$
20b-PbSe	**20b**-CdSe	3.5	2.7	2.0	2.0	0.89	1.00	$MgZn_2$
20p-Au	**20b**-CdSe	6.0	5.4	2.2	2.0	0.90	0.91	CuAu

[a]Inorganic diameter. [b]Thickness of the organic shell. [c]$(d_{small} + 2t_{small})/(d_{large} + 2t_{large})$. [d]$t_{small}/t_{large}$. [e]Two additional binary liquid crystalline phases are observed with this mixture.

DOI: 10.1021/jacs.6b04979
J. Am. Chem. Soc. 2016, 138, 10508−10515

in partnership with the University of Pennsylvania's NSF MRSEC under Award No. DMR-112090. C.B.M. acknowledges the Richard Perry University Professorship at the University of Pennsylvania.

REFERENCES

(1) Kovalenko, M. V.; Scheele, M.; Talapin, D. V. *Science* **2009**, *324* (5933), 1417.
(2) Dong, A.; Ye, X.; Chen, J.; Kang, Y.; Gordon, T.; Kikkawa, J. M.; Murray, C. B. *J. Am. Chem. Soc.* **2011**, *133* (4), 998.
(3) Nag, A.; Kovalenko, M. V.; Lee, J.-S.; Liu, W.; Spokoyny, B.; Talapin, D. V. *J. Am. Chem. Soc.* **2011**, *133* (27), 10612.
(4) Fafarman, A. T.; Koh, W.; Diroll, B. T.; Kim, D. K.; Ko, D.-K.; Oh, S. J.; Ye, X.; Doan-Nguyen, V.; Crump, M. R.; Reifsnyder, D. C.; Murray, C. B.; Kagan, C. R. *J. Am. Chem. Soc.* **2011**, *133* (39), 15753.
(5) Lewandowski, W.; Fruhnert, M.; Mieczkowski, J.; Rockstuhl, C.; Górecka, E. *Nat. Commun.* **2015**, *6*, 6590.
(6) Cseh, L.; Mang, X.; Zeng, X.; Liu, F.; Mehl, G. H.; Ungar, G.; Siligardi, G. *J. Am. Chem. Soc.* **2015**, *137* (40), 12736.
(7) Dintinger, J.; Tang, B.-J.; Zeng, X.; Liu, F.; Kienzler, T.; Mehl, G. H.; Ungar, G.; Rockstuhl, C.; Scharf, T. *Adv. Mater.* **2013**, *25* (14), 1999.
(8) Ye, X.; Zhu, C.; Ercius, P.; Raja, S. N.; He, B.; Jones, M. R.; Hauwiller, M. R.; Liu, Y.; Xu, T.; Alivisatos, A. P. *Nat. Commun.* **2015**, *6*, 10052.
(9) Kovalenko, M. V.; Bodnarchuk, M. I.; Talapin, D. V. *J. Am. Chem. Soc.* **2010**, *132* (43), 15124.
(10) Rowland, C. E.; Liu, W.; Hannah, D. C.; Chan, M. K. Y.; Talapin, D. V.; Schaller, R. D. *ACS Nano* **2014**, *8* (1), 977.
(11) Walker, B. J.; Nair, G. P.; Marshall, L. F.; Bulović, V.; Bawendi, M. G. *J. Am. Chem. Soc.* **2009**, *131* (28), 9624.
(12) Talapin, D. V.; Lee, J.-S.; Kovalenko, M. V.; Shevchenko, E. V. *Chem. Rev.* **2010**, *110* (1), 389.
(13) Cano, I.; Huertos, M. A.; Chapman, A. M.; Buntkowsky, G.; Gutmann, T.; Groszewicz, P. B.; van Leeuwen, P. W. N. M. *J. Am. Chem. Soc.* **2015**, *137* (24), 7718.
(14) Fleutot, S.; Nealon, G. L.; Pauly, M.; Pichon, B. P.; Leuvrey, C.; Drillon, M.; Gallani, J.-L.; Guillon, D.; Donnio, B.; Begin-Colin, S. *Nanoscale* **2013**, *5* (4), 1507.
(15) Murthy, S. K. *Int. J. Nanomed.* **2007**, *2* (2), 129.
(16) Peng, X.; Manna, L.; Yang, W.; Wickham, J.; Scher, E.; Kadavanich, A.; Alivisatos, A. *Nature* **2000**, *404* (6773), 59.
(17) Elghanian, R.; Storhoff, J. J.; Mucic, R. C.; Letsinger, R. L.; Mirkin, C. A. *Science* **1997**, *277* (5329), 1078.
(18) Mirkin, C. A.; Letsinger, R. L.; Mucic, R. C.; Storhoff, J. J. *Nature* **1996**, *382* (6592), 607.
(19) Nykypanchuk, D.; Maye, M. M.; van der Lelie, D.; Gang, O. *Nature* **2008**, *451* (7178), 549.
(20) Dolzhnikov, D. S.; Zhang, H.; Jang, J.; Son, J. S.; Panthani, M. G.; Shibata, T.; Chattopadhyay, S.; Talapin, D. V. *Science* **2015**, *347* (6220), 425.
(21) Boisselier, E.; Salmon, L.; Ruiz, J.; Astruc, D. *Chem. Commun.* **2008**, *44*, 5788.
(22) Jishkariani, D.; Diroll, B. T.; Cargnello, M.; Klein, D. R.; Hough, L. A.; Murray, C. B.; Donnio, B. *J. Am. Chem. Soc.* **2015**, *137* (33), 10728.
(23) Draper, M.; Saez, I. M.; Cowling, S. J.; Gai, P.; Heinrich, B.; Donnio, B.; Guillon, D.; Goodby, J. W. *Adv. Funct. Mater.* **2011**, *21* (7), 1260.
(24) Donnio, B.; García-Vázquez, P.; Gallani, J.-L.; Guillon, D.; Terazzi, E. *Adv. Mater.* **2007**, *19* (21), 3534.
(25) Kanie, K.; Matsubara, M.; Zeng, X.; Liu, F.; Ungar, G.; Nakamura, H.; Muramatsu, A. *J. Am. Chem. Soc.* **2012**, *134* (2), 808.
(26) Mischler, S.; Guerra, S.; Deschenaux, R. *Chem. Commun.* **2012**, *48* (16), 2183.
(27) Nguyen, T. T.; Albert, S.; Nguyen, T. L. A.; Deschenaux, R. *RSC Adv.* **2015**, *5* (35), 27224.
(28) Mirzaei, J.; Urbanski, M.; Kitzerow, H.-S.; Hegmann, T. *Philos. Trans. R. Soc., A* **2013**, *371* (1988), 20120256.
(29) Stamatoiu, O.; Mirzaei, J.; Feng, X.; Hegmann, T. In *Liquid Crystals: Materials Design and Self-Assembly*; Tschierske, C., Ed.; Topics in Current Chemistry; Springer-Verlag: Berlin, 2011; Vol. *318*, pp 331−393.
(30) Nealon, G. L.; Greget, R.; Dominguez, C.; Nagy, Z. T.; Guillon, D.; Gallani, J.-L.; Donnio, B. *Beilstein J. Org. Chem.* **2012**, *8*, 349.
(31) Lewandowski, W.; Wójcik, M.; Górecka, E. *ChemPhysChem* **2014**, *15* (7), 1283.
(32) Saliba, S.; Mingotaud, C.; Kahn, M. L.; Marty, J.-D. *Nanoscale* **2013**, *5* (15), 6641.
(33) Wójcik, M. M.; Olesińska, M.; Sawczyk, M.; Mieczkowski, J.; Górecka, E. *Chem. - Eur. J.* **2015**, *21* (28), 10082.
(34) Zep, A.; Wojcik, M. M.; Lewandowski, W.; Sitkowska, K.; Prominski, A.; Mieczkowski, J.; Pociecha, D.; Górecka, E. *Angew. Chem., Int. Ed.* **2014**, *53* (50), 13725.
(35) Kanayama, N.; Tsutsumi, O.; Kanazawa, A.; Ikeda, T. *Chem. Commun.* **2001**, *2001* (24), 2640.
(36) In, I.; Jun, Y.-W.; Kim, Y. J.; Kim, S. Y. *Chem. Commun.* **2005**, *6*, 800.
(37) Chico, R.; Castillejos, E.; Serp, P.; Coco, S.; Espinet, P. *Inorg. Chem.* **2011**, *50* (17), 8654.
(38) Travesset, A. *Proc. Natl. Acad. Sci. U. S. A.* **2015**, *112* (31), 9563.
(39) Gehringer, L.; Bourgogne, C.; Guillon, D.; Donnio, B. *J. Am. Chem. Soc.* **2004**, *126* (12), 3856.
(40) Iha, R. K.; Wooley, K. L.; Nyström, A. M.; Burke, D. J.; Kade, M. J.; Hawker, C. J. *Chem. Rev.* **2009**, *109* (11), 5620.
(41) Peng, Z. A.; Peng, X. *J. Am. Chem. Soc.* **2001**, *123* (1), 183.
(42) Hines, M. a.; Scholes, G. D. *Adv. Mater.* **2003**, *15* (21), 1844.
(43) Yu, W. W.; Falkner, J. C.; Shih, B. S.; Colvin, V. L. *Chem. Mater.* **2004**, *16* (17), 3318.
(44) Kim, B. H.; Lee, N.; Kim, H.; An, K.; Park, Y. Il; Choi, Y.; Shin, K.; Lee, Y.; Kwon, S. G.; Na, H. B.; Park, J.-G.; Ahn, T.-Y.; Kim, Y.-W.; Moon, W. K.; Choi, S. H.; Hyeon, T. *J. Am. Chem. Soc.* **2011**, *133* (32), 12624.
(45) Yang, Y.; Qin, H.; Jiang, M.; Lin, L.; Fu, T.; Dai, X.; Zhang, Z.; Niu, Y.; Cao, H.; Jin, Y.; Zhao, F.; Peng, X. *Nano Lett.* **2016**, *16* (4), 2133.
(46) Goodfellow, B. W.; Yu, Y.; Bosoy, C. A.; Smilgies, D.-M.; Korgel, B. A. *J. Phys. Chem. Lett.* **2015**, *6* (13), 2406.
(47) Travesset, A. *J. Chem. Phys.* **2014**, *141* (16), 164501.
(48) Boles, M. A.; Talapin, D. V. *J. Am. Chem. Soc.* **2015**, *137* (13), 4494.
(49) Shevchenko, E. V.; Talapin, D. V.; Kotov, N. A.; O'Brien, S.; Murray, C. B. *Nature* **2006**, *439* (7072), 55.
(50) Horst, N.; Travesset, A. *J. Chem. Phys.* **2016**, *144*, 014502.
(51) Travesset, A. *Soft Matter* **2016**, DOI: 10.1039/C6SM00713A.

DOI: 10.1021/jacs.6b04979
J. Am. Chem. Soc. 2016, 138, 10508−10515